

---

1    **The impact of organic nitrates on summer ozone formation in Shanghai,**  
2    **China**

3    Chunmeng Li<sup>1</sup>, Xiaorui Chen<sup>2,3\*</sup>, Haichao Wang<sup>2,3</sup>, Tianyu Zhai<sup>4</sup>, Xuefei Ma<sup>5</sup>, Xinping Yang<sup>4</sup>, Shiyi  
4    Chen<sup>5</sup>, Min Zhou<sup>6</sup>, Shengrong Lou<sup>6</sup>, Xin Li<sup>5</sup>, Limin Zeng<sup>5</sup>, Keding Lu<sup>5\*</sup>

5    <sup>1</sup> Center for Environmental Metrology, The National Institute of Metrology, Beijing 100029, China.

6    <sup>2</sup> School of Atmospheric Sciences, Sun Yat-sen University, Zhuhai, Guangdong, 519082, China.

7    <sup>3</sup> Guangdong Provincial Observation and Research Station for Climate Environment and Air Quality  
8    Change in the Pearl River Estuary, Key Laboratory of Tropical Atmosphere-Ocean System, Ministry  
9    of Education, Southern Marine Science and Engineering Guangdong Laboratory (Zhuhai), Zhuhai,  
10   519082, China.

11   <sup>4</sup> State Environmental Protection Key Laboratory of Vehicle Emission Control and Simulation,  
12   Chinese Research Academy of Environmental Sciences, Beijing, 100012, China

13   <sup>5</sup> State Key Joint Laboratory of Environmental Simulation and Pollution Control, The State  
14   Environmental Protection Key Laboratory of Atmospheric Ozone Pollution Control, College of  
15   Environmental Sciences and Engineering, Peking University, Beijing, 100871, China.

16   <sup>6</sup> State Environmental Protection Key Laboratory of the Cause and Prevention of Urban Air Pollution  
17   Complex, Shanghai Academy of Environmental Sciences, Shanghai, 200233, China.

18  
19   \* Correspondence: chenxr95@mail.sysu.edu.cn; k.lu@pku.edu.cn

20   **Abstract**

21   Organic nitrates serve as important secondary oxidation products in the atmosphere, playing a crucial  
22   role in the atmospheric radical cycles and influencing the production of secondary pollutants (ozone  
23   (O<sub>3</sub>) and secondary organic aerosols). However, field measurements of organic nitrates are scarce in  
24   China, and a comprehensive localized mechanism for organic nitrates is absent, hindering effective  
25   pollution mitigation strategies. In this study, we conducted measurements of ambient gaseous organic  
26   nitrates and examined their effects on local O<sub>3</sub> production at a polluted urban site in eastern China  
27   during summer. The average daytime concentrations of alkyl nitrates (ANs) and peroxy nitrates (PNs)  
28   throughout the campaign were 0.5±0.3 ppbv and 0.9±0.7 ppbv, respectively, with peaks reaching up to  
29   1.6 ppbv and 3.6 ppbv. An observation-constrained box model, incorporating an updated mechanism  
30   for organic nitrates, was employed to assess the environmental impact of these compounds. The model  
31   results indicated that PNs production inhibited the daytime O<sub>3</sub> production by 16% (0.8 ppbv/h), which  
32   is relatively low compared to previous studies. Furthermore, scenario analyses revealed that production  
33   yields ( $\alpha$ ) of ANs would alter the response of O<sub>3</sub> formation to precursors due to varying compositions  
34   of volatile organic compounds. Our results suggest that blind pollution control may cause ineffective  
35   pollution prevention and highlight the necessity of a thorough understanding on organic nitrate

### 36 chemistry for local O<sub>3</sub> control strategy.

37 1. Introduction

Tropospheric ozone, as an important oxidant, influences the atmospheric lifetimes of trace gases through its involvement in photochemical processes, thereby playing a crucial role in climate change and atmospheric chemistry. There is a broad consensus that high near-surface ozone concentrations are hazardous to human health and environmental ecosystems, particularly affecting the human respiratory and cardiovascular systems, and result in decreased yields of various crops (Ashmore, 2005; Xue and Zhang, 2023). A scientific assessment of tropospheric ozone is essential for the development of public health policies and for addressing long-term air pollution challenges (Monks et al., 2015). Primary pollutants, such as nitrogen oxides ( $\text{NO}_x$ ) and volatile organic compounds (VOCs), participate in the formation of  $\text{HO}_x$  radicals ( $\text{RO}_x = \text{RO}_2 + \text{HO}_2 + \text{OH}$ ) cycles and  $\text{NO}_x$  cycles under sunlight, leading to the continuous production of ozone as a secondary oxidation product within these cycles. In addition to the reaction between OH and  $\text{NO}_2$  that produces  $\text{HNO}_3$  as part of chain termination reactions, the interaction of  $\text{RO}_2$  and NO that produces organic nitrates is of increasing concern (Present et al., 2020). The atmospheric production of organic nitrates consumes both  $\text{NO}_x$  and  $\text{RO}_2$ . Therefore, the chemistry of organic nitrates will significantly influence the prevention and control of ozone, with  $\text{NO}_x$  and VOCs serving as independent variables.

Both anthropogenic activities and natural processes contribute to the emissions of  $\text{NO}_x$  and VOCs, which are produced from produce  $\text{RO}_2$  in the presence of oxidants such as OH. Subsequently,  $\text{RO}_2$  reacts with NO to yield  $\text{NO}_2$  and RO. After that,  $\text{NO}_2$  photolysis produces  $\text{O}_3$ , while RO is converted into  $\text{HO}_2$  through an isomerization reaction, thereby forming the ozone production cycle. Within the cycle, a branching reaction between  $\text{RO}_2$  and NO leads to the formation of alkyl nitrates ( $\text{RONO}_2$ , ANs), while  $\text{RO}_2$  may also react with  $\text{NO}_2$  to generate peroxy nitrates ( $\text{RO}_2\text{NO}_2$ , PNs). Given that PNs are prone to thermal dissociation near the surface (Roberts and Bertman, 1992), they can influence  $\text{O}_3$  production by modifying the availability of  $\text{NO}_x$  and  $\text{RO}_x$ . Due to the competitive production dynamics between PNs and  $\text{O}_3$ , numerous field observations and model simulations have been conducted to investigate the impact of peroxyacetyl nitrate (PAN) on  $\text{O}_3$  production (Liu et al., 2021; Zeng et al., 2019; Zhang et al., 2020). As another key secondary oxidation product, the branching ratio ( $\alpha$ ) for ANs formation varies between 0.1% and 35% (Perring et al., 2013). For ANs formation, the branching ratio ( $\alpha$ ), the reaction ratio  $k_{1b}/(k_{1a}+k_{1b})$ , varies between 0.1-35%, which are associated with the carbon chain structure of the molecule, the distribution of functional groups, temperature, and pressure (Reisen et al., 2005; Arey et al., 2001; Wennberg et al., 2018; Russell and Allen, 2005; Butkovskaya et al., 2012; Cassanelli et al., 2007). Some values of  $\alpha$ , which have not been quantified in the laboratory, are estimated through structure-activity relationships (Arey et al., 2001; Reisen et al., 2005; Teng et al., 2015; Yeh and Ziemann, 2014a; Yeh and Ziemann, 2014b). Multiple field observations revealed a strong linear correlation between ANs and  $\text{O}_3$ , with a correlation coefficient ( $r^2$ ) exceeding 0.5, further substantiating the competitive relationship between ANs and  $\text{O}_3$  (Aruffo et al., 2014; Day et al., 2003; Flocke et al., 1998).



76 Currently, research on the effects of ANs on O<sub>3</sub> distribution is predominantly located in Europe  
77 and the United States. Following the first in situ measurement of total organic nitrates through thermal

带格式的: 字体颜色: 文字 1

78 dissociation laser-induced fluorescence instrument (TD-LIF) by Day et al., field observations of total  
79 ANs have been continuously conducted to study the role of ANs in the nitrogen cycle (Aruffo et al.,  
80 2014; Browne et al., 2013; Chen et al., 2017; Darer et al., 2011; Day et al., 2003; Sadanaga et al., 2016).  
81 In conjunction with field observations and model simulations, Farmer et al. were the first to indicate  
82 that ANs influence the sensitivity of NO<sub>x</sub>-VOCs-O<sub>3</sub> (Farmer et al., 2011). As NO<sub>x</sub> emissions decrease  
83 due to pollution control measures, ANs chemistry is expected to play an increasingly significant role  
84 in O<sub>3</sub> simulations (Present et al., 2020; Zare et al., 2018). Current mechanisms for O<sub>3</sub> simulations  
85 generally achieve reasonable predictions in large-scale models; however, they exhibit deviations  
86 exceeding 10 ppbv in regional simulations (Young et al., 2018). Subsequent studies have demonstrated  
87 that refining the ANs chemistry can further improve the simulation performance for O<sub>3</sub> (Schwantes et  
88 al., 2020). ANs are predominantly produced through oxidation reactions facilitated by OH, O<sub>3</sub>, and  
89 NO<sub>3</sub>. The daytime ANs are mainly contributed by the OH channel, whereas during nighttime, the  
90 contribution of the NO<sub>3</sub> channel is linked to significantly increased yields of ANs (Liebmann et al.,  
91 2018; Ng et al., 2017; Zare et al., 2018). Presently, the enhancement of ANs chemistry mainly focuses  
92 on BVOCs, particularly isoprene and monoterpenes. These researches aim to enhance the yield of ANs  
93 derived from BVOCs, the re-release ratio of ANs to NO<sub>x</sub>, and the contribution of ANs to aerosols  
94 (Fisher et al., 2016; Romer et al., 2016; Travis et al., 2016; Zare et al., 2018). Despite the establishment  
95 of a complete mechanism scheme at present, significant uncertainties remain in ANs simulation, which  
96 may introduce substantial uncertainties into the O<sub>3</sub> simulation.

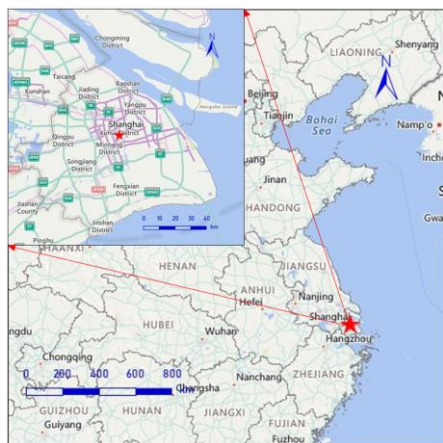
97 Atmospheric pollution is common across China, particularly in the Yangtze River Delta. Shanghai,  
98 as a highly urbanized metropolis in the Yangtze River Delta, has rendered the region's complex  
99 pollution due to its rapid economic growth and urbanization (Wang et al., 2022; Zhu et al., 2021).  
100 Previous studies have shown a significant increase in near-surface O<sub>3</sub> levels from 2006 to 2016 in  
101 Shanghai (Gao et al., 2017). However, research on the ANs chemistry and their impact on O<sub>3</sub> pollution  
102 remains limited in this area. In addition, most field measurements of ANs have focused on short-chain  
103 species (Ling et al., 2016; Song et al., 2018; Sun et al., 2018; Wang et al., 2013), which have been  
104 observed to exert a typical inhibition effect on daytime O<sub>3</sub> production. A limited number of total ANs  
105 measurements found that both ANs and O<sub>3</sub> production were in the VOC-limited regime (Li et al., 2023).  
106 To further investigate the influence of organic nitrates on O<sub>3</sub> production, this study describes the  
107 distribution of organic nitrates based on a comprehensive field campaign conducted in Shanghai,  
108 analyzes the effects of organic nitrates on O<sub>3</sub> production through model simulations, and offers  
109 recommendations for the prevention and control of ozone pollution in the region.

## 110 2. Methodology

### 111 2.1 Measurement site and instrumentations

112 A comprehensive campaign was conducted in Shanghai to further investigate the chemical  
113 behavior of organic nitrates in urban environments across China. As depicted in Fig. 1, the site is  
114 located in the Xuhui District of Shanghai (121.44°E, 31.18°N), in proximity to the Shanghai Inner  
115 Ring Viaduct, surrounded by numerous residential and office areas without significant industrial  
116 emission sources. The site is mainly influenced by morning-evening rush hours, as well as the transport  
117 of air masses to the urban location. The overall wind speed was low, predominantly originating from

118 the east. All the measurement instruments were housed in the temperature-controlled room within the  
119 laboratory building at the Shanghai Academy of Environmental Sciences. Thermal Dissociation-  
120 Cavity Enhanced Absorption Spectroscopy (TD-CEAS) was positioned on the 7th floor about 25 m  
121 above ground level, with the sampling tube extending out through the window.



122

123 **Figure 1.** Map of the city of Shanghai and the surrounding area (@ MeteoInfoMap). The red star is the location of  
124 the campaign site.

125 The Shanghai campaign focused on studying summer ozone pollution, with the chemical  
126 parameters presented in Table 1. Organic nitrates were measured by TD-CEAS with a sampling flow  
127 rate of 3 L/min and a sampling duration of 3 min for alternating measurements of NO<sub>2</sub>, PNs, and ANs.  
128 The sampling apparatus consisted of a 2-meter-long 1/4-inch tetrafluoroethylene (TFE) tube, through  
129 which the atmosphere was filtered through a TFE particulate filter. The membrane was replaced once  
130 a day to mitigate the interference caused by wall loss. The measurement of PAN was conducted by gas  
131 chromatography electron capture detection (GC-ECD). The Measurement of N<sub>2</sub>O<sub>5</sub> was performed via  
132 CEAS, which relies on the thermal dissociation of N<sub>2</sub>O<sub>5</sub> to yield NO<sub>3</sub>. Particulate nitrates and gaseous  
133 HNO<sub>3</sub> were measured online by AeRosols and GAses (MARGA), where soluble substances were  
134 quantified through ion chromatography following dissolution. The measurements of HONO were  
135 finished by CEAS during the campaign. Measurements of VOCs were achieved using a combination  
136 of GC-FID and GC-MS, with GC-MS predominating due to the limited species measured by GC-FID.  
137 The photolysis rate constant (J value) was determined using a spectrum radiometer with a time  
138 resolution of 20 s. Additionally, simultaneous measurements of other trace gases such as NO, NO<sub>2</sub>,  
139 SO<sub>2</sub>, CO, O<sub>3</sub>, and PM<sub>2.5</sub> were conducted using commercial instruments.

140 **Table 1.** Measured species for organic nitrates analysis and instrument time resolution, accuracy, and detection  
141 limitation.

Parameters	Measurement technique	Time resolution	Accuracy	Detection limit
ANs, PNs, NO <sub>2</sub>	TD-CEAS	3 min	± 8%	93 pptv
PAN	GC-ECD	5 min	± 10%	5 pptv

---

$\text{N}_2\text{O}_5$	CEAS	1 min	$\pm$ 19%	2.7 pptv
NO	Thermo 42i	1 min	$\pm$ 10%	60 pptv
$\text{NO}_2$	Chemiluminescence	1 min	$\pm$ 10%	300 pptv
HONO	CEAS	1 min	$\pm$ 3%	100 pptv
Particulate nitrate	2060 MARGA	1 h	$\pm$ 3%	$0.01 \mu\text{g}/\text{m}^3$
$\text{HNO}_3$	2060 MARGA	1 h	$\pm$ 3%	$0.01 \mu\text{g}/\text{m}^3$
$\text{SO}_2$	Thermo 43i-TLE	1 min	$\pm$ 16%	50 pptv
HCHO	Hantsch fluorimetry	1 min	$\pm$ 5%	25 pptv
CO	Thermo 48i-TLE	1 min	$\pm$ 16%	50 pptv
$\text{O}_3$	Thermo 49i	1 min	$\pm$ 5%	0.5 ppbv
$\text{PM}_{2.5}$	Thermo TEOM	1 min	$\pm$ 5%	$0.1 \mu\text{g}/\text{m}^3$
VOCs	GC-FID/GC-MS	1 h	$\pm$ 30%	20-300 pptv
J value	Spectrum radiometer	20 s	$\pm$ 10%	$5 \times 10^{-5} \text{ s}^{-1}$

---

142

143 **2.2 Model calculation**

144 To investigate the impact of ANs chemistry on  $\text{O}_3$  production, a box model was employed to  
 145 simulate the photochemistry processes. The mechanism of the model was enhanced based on RACM2  
 146 (Regional Atmospheric Chemical Mechanism version 2). This box model simulates the  
 147 physicochemical processes occurring within a defined volume for each reactant. It utilizes measured  
 148 parameters as the boundary condition to simulate the chemistry process while allowing for convenient  
 149 adjustments to the mechanism. The model generates files detailing concentration changes, budget  
 150 processes, and reaction rates, thereby providing an efficient means to simulate ground-level pollutants.  
 151 In this study, the box model was constrained by various parameters, including J values,  $\text{O}_3$ , NO,  $\text{NO}_2$ ,  
 152 CO, HONO, VOCs, RH, temperature, and pressure, with the time step set to 1h. The deposition process  
 153 was quantified using the deposition rate and the boundary layer height, with the dry deposition rate  
 154 established at 1.2 cm/s and the boundary layer height constrained by data obtained from NASA.

155 The RACM2 facilitates classification through the distribution of functional groups and  
 156 subsequently delineates reactions involving 17 stable non-organic compounds, 4 inorganic  
 157 intermediates, 55 stable organic compounds, and 43 intermediate organic species within the  
 158 mechanism. However, the mechanism description for ANs is notably abbreviated. The various ANs,  
 159 characterized by differing functional groups, are treated as a unified entity, thereby neglecting the  
 160 influence of functional groups on the underlying chemistry. Consequently, this study builds on the  
 161 previous research and further evaluates the updates of the mechanism (Li et al., 2023). These  
 162 mechanistic updates are developed based on the work of Zare et al. and primarily encompasses the  
 163 oxidation processes of BVOCs by OH and  $\text{NO}_3$ , as well as the deposition and the aerosol uptake, which  
 164 are detailed in the SI (Zare et al., 2018). Accordingly, three mechanistic schemas are compared based  
 165 on the campaign, which will be elaborated upon in subsequent sections. A box model based on the  
 166 above mechanism is used to calculate the ozone production rate ( $\text{P}(\text{O}_3)$ ) (Tan et al., 2017b).  $\text{P}(\text{O}_3)$  was  
 167 quantified based on the net production rate of  $\text{O}_x$  (the sum of  $\text{O}_3$  and  $\text{NO}_2$ ), by subtracting the  $\text{O}_x$   
 168 depletion from the instantaneous  $\text{O}_x$  production. The simulation uncertainty of the box model is about  
 169 40%, introduced mainly by the simplified reaction rate constants, photolysis rate constants, and near-

170 ground deposition (Lu et al., 2013). The impact of PNs photochemistry on local ozone is quantified by  
171 comparing the difference of the daytime P(O<sub>3</sub>) between the scenarios with and without PNs  
172 photochemistry via a chemical box model. Here, the PNs photochemistry includes the production and  
173 removal of PAN, MPAN and PPN.

174 To facilitate the assessment of the impacts of ANs on local O<sub>3</sub> pollution, we further conducted a  
175 simplified box model based on the steady-state assumption approach. Several studies have examined  
176 the combined effect of  $\alpha$  and VOCs reactivity on local O<sub>3</sub> levels using this approach (Farmer et al.,  
177 2011; Present et al., 2020; Romer et al., 2016; Romer et al., 2018). Briefly, the production pathway of  
178 ANs is simplified according to VOCs categories and the production rate of OH and HO<sub>2</sub>(P(HO<sub>x</sub>)) is  
179 fixed to a constant value. VOCs are categorized into two primary groups: non-oxygenated VOCs  
180 (RVOCs) and oxygenated VOCs (OVOCs). Both categories of VOCs undergo oxidation by OH,  
181 resulting in the formation of RO<sub>2</sub>, specifically RVOCRO<sub>2</sub> and OVOCRO<sub>2</sub>. The interaction between  
182 RVOCRO<sub>2</sub> and NO will produce  $\alpha$  ANs, (1- $\alpha$ ) NO<sub>2</sub>, HO<sub>2</sub>, and OVOC. Conversely, the reaction of  
183 OVOCRO<sub>2</sub> with NO directly generates NO<sub>2</sub>. In the Beijing-Tianjin-Hebei, Yangtze River Delta, and  
184 Chengdu-Chongqing regions of China, P(HO<sub>x</sub>) is approximately 4 ppbv/h (Lu et al., 2013; Tan et al.,  
185 2018a; Tan et al., 2018b). P(HO<sub>x</sub>) is therefore assumed to be 4 ppbv/h, with equal production rates of  
186 OH and HO<sub>2</sub>. The model also incorporates additional processes, including inter- and self-reactions of  
187 RO<sub>2</sub>, as well as reactions between NO<sub>2</sub> and NO, and deposition processes. In addition, during the  
188 daytime, NO is determined by j(NO<sub>2</sub>), O<sub>3</sub>, and NO<sub>2</sub> according to the photo-stationary state among NO-  
189 NO<sub>2</sub>-O<sub>3</sub>. Based on the above simplified approach, production rates of ANs and O<sub>3</sub> in this study can be  
190 derived by direct calculations.

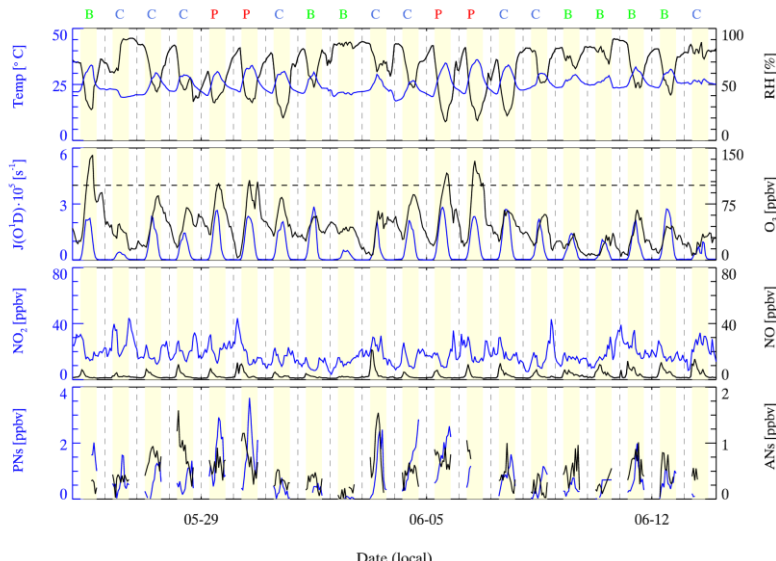
191 To investigate the effects of NO<sub>x</sub> and VOCs on O<sub>3</sub> production, the theoretical maximum of P(O<sub>3</sub>)  
192 was simulated by a box model under varying concentrations of NO<sub>x</sub> and VOCs. This approach was  
193 employed to develop an empirical kinetic modeling approach for ozone production (EKMA). The  
194 EKMA serves as a model sensitivity method to inform strategies for pollutant abatement. In this study,  
195 EKMA utilizes the measured mean parameters as the initial point. Each parameter was incrementally  
196 adjusted in 30 equidistant steps to create scaled arrays of VOCs and NO<sub>x</sub>, which were subsequently  
197 used to simulate the variations in P(O<sub>3</sub>) resulting from changes in precursor concentrations. Ultimately,  
198 contour plots illustrating the relationship between P(O<sub>3</sub>) arrays versus the concentrations of NO<sub>x</sub> and  
199 VOCs are plotted based on the simulation results.

### 200 3. Results and discussions

#### 201 3.1 Overview of organic nitrates and precursors

202 The duration of the Shanghai campaign was 20 days, spanning from May 25 to June 13, 2021.  
203 The analysis of organic nitrates is performed from 6 a.m. to 6 p.m., as measurements taken during  
204 nighttime were subject to interference from N<sub>2</sub>O<sub>5</sub> and its derivatives, a phenomenon noted in previous  
205 studies (Li et al., 2021; Li et al., 2023). Simultaneous measurements of PAN and PNs were conducted  
206 throughout the campaign. There was a malfunction of the GC-ECD instrument from June 12 to June  
207 13, during which the measurements of PAN were generally low. Relative humidity (RH) varied  
208 considerably, with over 95% during rainfall periods on June 2, June 9, June 10, and June 13, while the  
209 remaining days were predominantly sunny. Temperatures were high, with minimums of 20 °C and

210 daytime peaks reaching up to 36 °C. The wind speeds were generally high during the daytime and low  
211 at night, with maximum of 4.2 m/s. The easterly winds prevailed during the campaign, except for May  
212 27-28 and June 3-6 with mostly west and southwest winds.



213  
214 **Figure 2.** The time series of the related parameters focused on organic nitrates during the campaign. The background  
215 days are represented by green B, the clean days are represented by blue C, and the ozone pollution day is represented  
216 by red P.

217 According to Chinese air quality standards for Class II areas, which define ozone pollution days  
218 as those with an hourly average exceeding 100 ppbv, the periods from May 29 to May 30 and June 5  
219 to June 6 have been identified as ozone pollution days. The remaining days were without ozone  
220 pollution and categorized as either clean or background days based on the observed daily. For clean  
221 days, parameters, including  $K_{OH}$ ,  $SO_2$ , and  $CO$ , show significant diurnal variations in  $K_{OH}$  and  $CO$  (Fig  
222 S1), and no rain occurs. The days that are neither ozone pollution days nor clean days are then classified  
223 as background days. The daytime averages of environmental parameters during the ozone pollution  
224 period, the clean period, and the background period are presented in Table 2. Excluding cloudy and  
225 rainy days, the daytime peak of  $J(O^1D)$  was near  $2.8 \times 10^5 \text{ s}^{-1}$ , indicating a high photochemical oxidation  
226 potential. As a secondary photochemical product,  $O_3$  exhibited a typical daily profile, peaking at 140.5  
227 ppbv throughout the campaign. The measurements of PNs peaked at 3.6 ppbv with a daytime average  
228 of  $0.5 \pm 0.3$  ppbv, while ANs peaked at 1.6 ppbv with a daytime average of  $0.5 \pm 0.3$  ppbv. Ozone  
229 pollution periods were often associated with high organic nitrates. The mean daily variation of  $NO_x$   
230 was consistent with the characteristics of typical urban sites, significantly influenced by the morning-  
231 evening rush hours. During the daytime, NO exhibited a single peak distribution, whereas  $NO_2$   
232 displayed a bimodal distribution. In comparison to the background and clean period, the ozone  
233 pollution period was characterized with higher temperatures and lower humidity. Additionally, the  
234 photolysis rate and levels of  $PM_{2.5}$  were both elevated during pollution days.

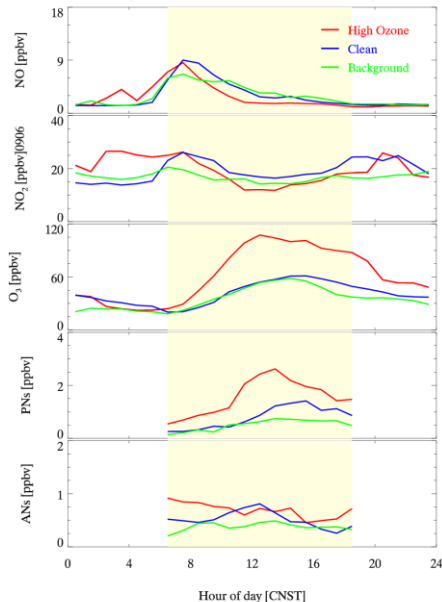
带格式的: 字体颜色: 文字 1  
带格式的: 字体颜色: 文字 1

235 **Table 2.** Summary of daytime averages of chemical parameters over different periods during the Shanghai campaign.

Phase	Ozone pollution	Background	Clean
T/°C	29.8±3.7	27.0±3.4	26.0±3.5
P/hPa	1043.6±0.8	1045.3±0.9	1044.3±1.4
RH/%	39.2±13.9	65.2±16.0	62.4±17.2
J(O <sup>1</sup> D)×10 <sup>5</sup> /s	1.3±0.9	0.9±0.8	0.8±0.8
J(NO <sub>2</sub> )×10 <sup>3</sup> /s	4.5±2.1	2.8±2.0	2.6±1.9
NO <sub>2</sub> /ppbv	17.3±6.1	16.5±5.8	20.3±7.4
NO/ppbv	3.2±2.6	4.0±2.7	4.2±3.7
O <sub>3</sub> /ppbv	78.6±30.9	41.6±27.7	45.0±21.5
PM <sub>2.5</sub> /μg·m <sup>-3</sup>	25.9±4.3	18.3±13.4	21.9±10.0
SO <sub>2</sub> /ppbv	2.2±1.7	0.4±0.5	0.6±0.7
CO/ppbv	505.3±64.3	441.6±133.3	535.0±147.8
ISO/ppbv	0.1±0.1	0.2±0.2	0.1±0.1

236

237 The mean diurnal profiles of organic nitrates and related parameters observed during the campaign  
 238 are shown in Fig. 3. During the ozone pollution period, NO<sub>x</sub> exhibited a peak concentration at 3:00  
 239 a.m., indicating the transport of a polluted air mass to the site. In comparison to the clean period,  
 240 daytime NO<sub>x</sub> was lower during the ozone pollution period, particularly at noon when NO dropped to  
 241 as low as 1.7 ppbv. Correspondingly, ANs during the ozone pollution period were generally high, but  
 242 the daily variation was not significant. Therefore, the sources of ANs were more complex during the  
 243 ozone pollution period, involving both transport contribution and local production, which aligns with  
 244 the significantly increased background O<sub>3</sub>. During the clean period, the daytime peak of O<sub>3</sub> was notably  
 245 reduced and occurred later in the day. The fluctuations in NO<sub>x</sub> were more closely associated with  
 246 morning and evening rush hours. The daytime peak of PNs decreased from 2.6 ppbv to 1.4 ppbv. In  
 247 addition, the diurnal profile of ANs displayed a more pronounced peak at noon. During the background  
 248 period, there was a further decline in the daytime peaks of NO<sub>x</sub> compared to the clean period. The  
 249 diurnal profile of O<sub>3</sub> exhibited similar trends, but the duration of high O<sub>3</sub> was significantly shortened.  
 250 The levels of both PNs and ANs exhibited a decline, approaching the background concentrations.



251

252 **Figure 3.** Mean diurnal profiles of organic nitrates and related parameters during different observation periods.

253 Here, we compare our observations ~~to with~~ the study previously conducted in Xinjin, which is a  
 254 ~~suburban site~~, located in basin topography and faces emerging ozone pollution recently, to determine  
 255 the effect of organic nitrate on  $O_3$  production under different pollution conditions (Li et al., 2023). The  
 256 Shanghai and Xinjin campaigns were conducted in early and late summer, respectively, exhibiting  
 257 similar meteorological conditions. Photochemical conditions during both two campaigns are  
 258 comparable, with the daily means of  $J(O^1D)$  were  $0.9 \times 10^{-5} \text{ s}^{-1}$  and  $0.8 \times 10^{-5} \text{ s}^{-1}$ , while the daily means  
 259 of  $J(NO_2)$  were  $3.1 \times 10^{-3} \text{ s}^{-1}$  and  $3.0 \times 10^{-3} \text{ s}^{-1}$ , respectively, during Shanghai and Xinjin campaigns.  
 260 The ratio of NO to  $NO_2$  was 0.19 and 0.17 at Shanghai and Xinjin, respectively. Meanwhile, the  
 261 concentration of  $NO_x$  observed in Shanghai site (daily averages of 22.0 ppbv) is higher than that  
 262 observed in Xinjin site (daily averages of 12.5 ppbv). The concentrations of  $SO_2$  and  $CO$  at Shanghai  
 263 site were 0.9 and 491.4 ppbv, while  $SO_2$  and  $CO$  were 0.6 and 404.5 ppbv, respectively. Therefore, the  
 264 air masses at Shanghai site were less aged than Xinjin site. However, the concentration of VOCs is  
 265 lower in Shanghai campaign compared to Xinjin campaign, with daily mean of 23.5 ppbv compared  
 266 to 22.4 ppbv. Therefore, a comparison of the two campaigns facilitates a comprehensive analysis of  
 267 the impacts of organic nitrate chemistry on local ozone pollution.

带格式的: 字体颜色: 文字 1  
 带格式的: 字体颜色: 文字 1  
 带格式的: 字体颜色: 文字 1

268 **3.2 Evaluation of organic nitrates simulations**

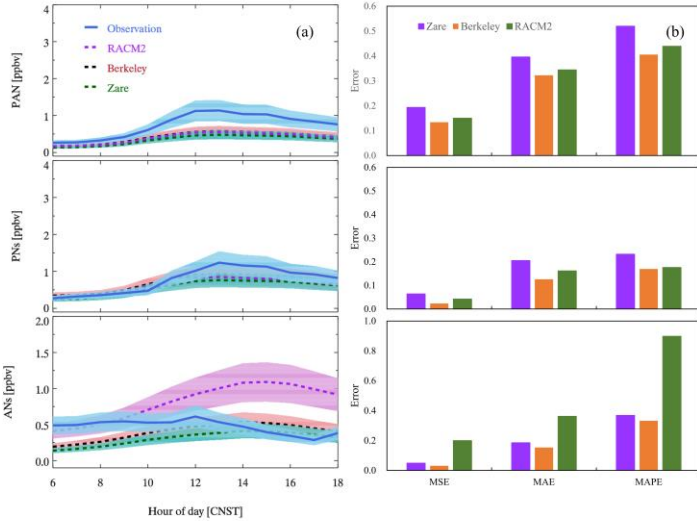
269 In light of the updates to the mechanisms, validation testing has been conducted. Our previous  
 270 study of the Xinjin campaign evaluated three mechanism schemes: mechanism S0, which is based on  
 271 RACM2, mechanism S1 and mechanism S2 which refines the budget for BVOC-derived organic

272 nitrates (Li et al., 2023). It was found that the performance of mechanism S2 for organic nitrates  
273 exhibited an improvement exceeding 50%. Mechanism S2 has been updated by the Berkeley group  
274 (Fisher et al., 2016; Travis et al., 2016), which includes enhancements to the production mechanism of  
275 isoprene, the incorporation of the production mechanism for monoterpenes, and the completion of the  
276 uptake of organic nitrates by aerosols. Additionally, the Zare mechanism further refines the production  
277 mechanism of organic nitrates initiated by OH and  $\text{NO}_3$ , as well as improving the deposition process  
278 of organic nitrates. As a result, the Shanghai campaign was simulated using RACM2, Berkeley, and  
279 Zare mechanisms respectively for comparison.

280 The simulation result of organic nitrates under the three mechanisms is shown in Fig. 4a. The  
281 simulations for PAN~~or~~PNs exhibit an overall underestimation tendency, with the simulation of PAN  
282 demonstrating an even greater underestimation. Notably, the measured PN remained above 500 pptv  
283 during nighttime, indicating a continuous transportation contribution at this site. Furthermore, the  
284 underestimation of PN may be attributed to the unidentified  $\text{RO}_x$  sources. It is consistent with the  
285 findings from summer campaigns in Wangdu, Beijing, where an underestimation of  $\text{RO}_2$  was noted,  
286 particularly pronounced at elevated ambient  $\text{NO}_x$  (Tan et al., 2017a). In terms of ANs, the simulation  
287 performances vary across different mechanisms. A significant overestimation of ANs is evident when  
288 utilized RACM2. Conversely, the simulation based on the Berkeley and Zare mechanisms generally  
289 results in an underestimation of ANs, while the underestimation of the Zare mechanism is more  
290 significant. Sensitivity tests conducted in Xinjin campaign suggested that the simple representation of  
291 ANs uptake caused the underestimation (Li et al., 2023), which is the same reason of underestimation  
292 in the Shanghai campaign. The uptake of ANs need further experimental data to achieve a detailed  
293 description to support the simulations.

294 The diurnal profile of simulated PN is consistent with the measurements, both reaching their  
295 daytime peak shortly after sunrise. However, it is noteworthy that the peak concentration of PN  
296 measurements is significantly higher than the simulation. In a similar pattern with PN, the simulated  
297 ANs began to accumulate around 6:00 a.m. The measured ANs reached their peak near noon, whereas  
298 the simulations peaked at 3:00 pm. To evaluate the performance of simulations, as showed in Fig. 4b,  
299 three types of error ratios were calculated: Mean Square Error (MSE), Mean Absolute Error (MAE),  
300 and Mean Absolute Percentage Error (MAPE). Different error metrics for the organic nitrates exhibit  
301 a similar trend. The simulation performances of the Berkeley mechanism are better than the other two  
302 mechanisms. It should be noted that the Berkeley mechanism failed to fully reproduce the diurnal  
303 pattern of observed ANs. This is mainly due to the atmospheric transport that contributes to the ANs  
304 as mentioned in section 3.1. In addition, the drastic changes in  $\text{NO}_x$  during rush hours will introduce  
305 errors to the ANs measurements. In addition, the Zare mechanism refined the oxidation of BVOCs by  
306 OH or  $\text{NO}_3$  by introducing extra species with uncertain yields, which might bring biases to the  
307 simulations under high  $\text{NO}_x$  and anthropogenic VOCs. In general, the Berkeley mechanism performs  
308 better on simulation of ANs than Zare mechanism. As a result, the subsequent analysis is based on the  
309 Berkeley mechanism.

带格式的: 字体颜色: 文字 1

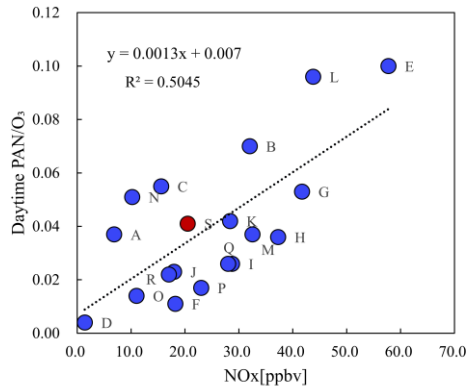


310

311 **Figure 4.** Mean diurnal profiles of observed and simulated ANs and PNs under different mechanism constraints  
 312 during the Shanghai campaign (a), and the error of the different cases (b), including mean square error (MSE), mean  
 313 absolute error (MAE) and mean absolute percentage error (MAPE).

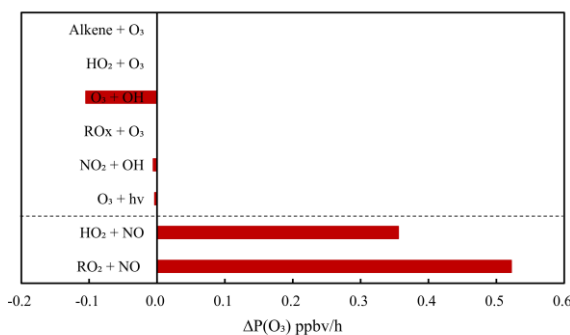
314 **3.3 Impact of PNs chemistry on local ozone production**

315      Organic nitrates and  $O_3$  have common precursors, and therefore the atmospheric behavior of  
 316 organic nitrates has an important influence on the local  $O_3$  distribution. The production of PNs  
 317 consumes  $NO_2$  and  $RO_x$ , thereby directly impacting  $O_3$  production. The relationship between the  
 318 distribution of PNs and  $O_3$  is examined throughout the campaign. Observed  
 319 PAN and O<sub>3</sub> between 9:00 a.m. and 2:00 p.m. are selected for the analysis to mitigate interference from  
 320 sources that are not produced during daytime. The correlation of PAN and PNs and with O<sub>3</sub> are shown  
 321 in Fig. S+S2. Both PAN and PNs demonstrate a strong correlation with O<sub>3</sub> with the ratio of PAN and  
 322 PNs to O<sub>3</sub> being 0.041 or 0.058. High ratios of PNs and O<sub>3</sub> usually indicate severe pollution episodes  
 323 (Shepson et al., 1992; Sun et al., 2020; Zhang et al., 2023; Zhang et al., 2014). The minimum ratio of  
 324 PAN/PNs and to O<sub>3</sub> (0.024) was found during the clean periods, which can be regarded as the threshold  
 325 for local photochemical pollution. NO<sub>x</sub> is the key pollutant for production of O<sub>3</sub> and PNs, in order to  
 326 study the relationship between the ratio of PAN and PNs to O<sub>3</sub> and NO<sub>x</sub>. The daytime ratios of PAN to  
 327 O<sub>3</sub> derived from historical field observations are summarized with corresponding NO<sub>x</sub> concentrations  
 328 in Fig. 5. The ratio derived from this study was distributed in the medium level of historical  
 329 observations. The linear correlation of NO<sub>x</sub> and the ratio of PAN to O<sub>3</sub> ratio suggests that the NO<sub>x</sub>  
 330 concentration controls the relative production of PNs and O<sub>3</sub>.



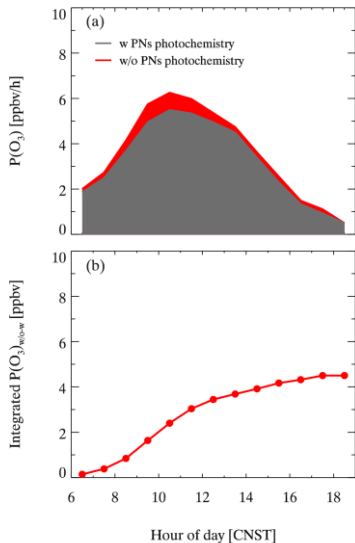
331  
 332 **Figure 5.** The relationship between historical daytime ratio of PAN to O<sub>3</sub> and NO<sub>x</sub> concentrations. The red dot is the  
 333 Shanghai campaign, and the blue dots are the historical campaigns. A: Grosjean et al., 2002 (Grosjean et al., 2002);  
 334 B: Lee et al., 2008 (Lee et al., 2008); C: Zhang et al., 2014 (Zhang et al., 2014); D-E: Zhang et al., 2009 (Zhang et  
 335 al., 2009); F-G: Zeng et al., 2019 (Zeng et al., 2019); H-K: Zhang et al., 2019 (Zhang et al., 2019); L-M: Sun et al.,  
 336 2020 (Sun et al., 2020); N: Li et al., 2023 (Li et al., 2023); O-R: Xu et al., 2024 (Xu et al., 2024); S: this study.

337 Sensitivity tests were conducted based on the box model to quantify the impact of PN  
 338 photochemistry on O<sub>3</sub> budgets. The differences of each pathway rate are calculated at the peak of O<sub>3</sub>  
 339 production rate (Fig. 6). In the absence of PN chemistry, two primary source pathways -namely, the  
 340 reaction between RO<sub>2</sub> and NO, and the reaction between HO<sub>2</sub> and NO-exhibit large enhancements of  
 341 0.52 and 0.36 ppbv/h, respectively. In comparison, O<sub>3</sub> sinks increase slightly in the absence of PN  
 342 photochemistry, with the reaction between OH and O<sub>3</sub> showing the most significant enhancement of  
 343 0.11 ppbv/h. Therefore, during the Shanghai campaign, PN photochemistry suppressed daytime ozone  
 344 production mainly by reducing the reaction between HO<sub>2</sub> or RO<sub>2</sub> and NO.



345  
 346 **Figure 6.** The simulated difference of ozone production rate ( $\Delta P(O_3)$ ) at 11am between the constraint of the PN  
 347 photochemistry and without the PN photochemistry.

348 The PNs maintain a notable concentration until 6:00 p.m., suggesting a persistent impact on local  
349 ozone production. As shown in Fig. 7a, the PNs photochemistry began to inhibit ozone production as  
350 early as 6 a.m. and increased up to 0.8 ppbv/h (16%) at 10 a.m. ~~The integrated inhibition of PNs  
351 photochemistry on ozone production was 4.5 ppbv during the Shanghai campaign (Fig. 7b), which was  
352 less pronounced than the Xinjin campaign. The reduced inhibition can be attributed to the lower P(PNs)  
353 observed in the Shanghai campaign (Fig. S2), where the maximum daytime PNs production rate was  
354 0.89 ppbv/h much lower than that in Xinjin campaign (3.09 ppbv/h). Therefore, the impact of PNs  
355 photochemistry on ozone production is closely linked to the PNs production, which should be  
356 elucidated through comprehensive simulation studies. The integrated inhibition of PNs photochemistry  
357 on O<sub>3</sub> production was 4.5 ppbv in the Shanghai campaign (Fig. 7b), which was less pronounced than  
358 the Xinjin campaign (20 ppbv). The reduced inhibition can be attributed to the lower PNs production  
359 rate (P(PNs)) observed in the Shanghai campaign (Fig. S3), where the maximum daytime P(PNs) was  
360 0.89 ppbv/h, much lower than that in Xinjin campaign (3.09 ppbv/h). In addition, the two campaigns  
361 had similar concentrations of VOCs, but daytime average of NO<sub>x</sub> in Shanghai site is 22.0 ppbv, which  
362 is much higher than that of Xinjin site (10.2 ppbv). The PNs formation would be reduced under high  
363 NO<sub>x</sub> condition due to the rapid termination reaction via OH and NO<sub>2</sub>, and thus limited the suppression  
364 effect of PNs formation which is the case in Shanghai campaign. Like in Xinjin campaign, PAN  
365 chemistry suppressed O<sub>3</sub> formation at a rate of 2.84 ppbv/h at a suburban site in Hong Kong (Zeng et  
366 al., 2019). However, it was reported that PAN tended to suppress O<sub>3</sub> production under low-NO<sub>x</sub> and  
367 low-RO<sub>x</sub> conditions but enhanced O<sub>3</sub> production with sufficient NO<sub>x</sub> at a rural coastal site in Qingdao,  
368 which is consistent with the comparison of Xinjin and Shanghai campaigns (Liu et al., 2021). The  
369 impacts of PNs photochemistry on O<sub>3</sub> vary across different days. As shown in Fig. S4, the integrated  
370 P(O<sub>3</sub>) change reaches 6.9 ppbv due to PNs photochemistry during ozone pollution period. For the  
371 background and clean periods, the changes are close to each other with a value of 3.8 and 4.2 ppbv,  
372 respectively. Therefore, the PNs photochemistry contributes to more P(O<sub>3</sub>) inhibition during the ozone  
373 pollution period, which should be considered in ozone pollution prevention.~~

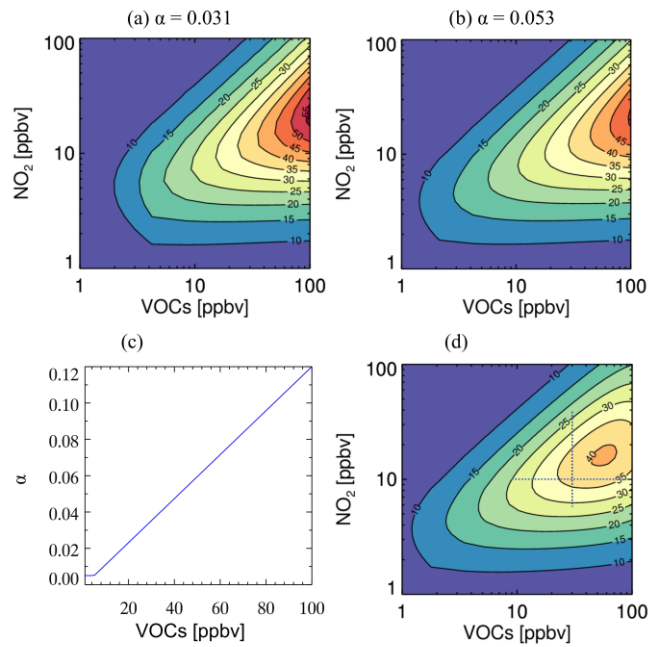


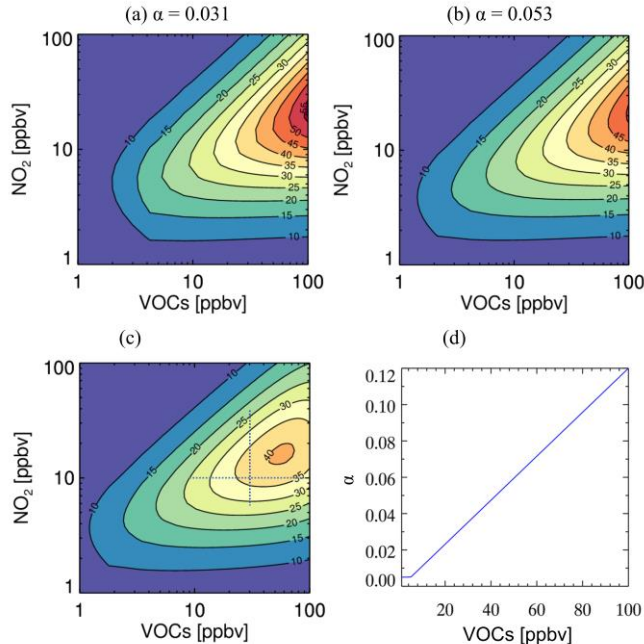
374

375 **Figure 7.** The impact of PN photochemistry on  $P(O_3)$  during the Shanghai campaign (a) daily changes of  $P(O_3)$   
 376 under the constraint of PN photochemistry, (b) integrated  $P(O_3)$  change constrained by PN photochemistry.

377 **3.4 Impact of ANs chemistry on local ozone production**

378 To elucidate the impact of the  $\alpha$  on  $O_3$  production, the EKMA was utilized to investigate the  
 379 combined response of  $NO_x$  and VOCs to  $O_3$  production at different  $\alpha$ . The  $O_3$  production was calculated  
 380 by a simplified approach in method 2.2 and the  $\alpha$  values were derived from weighted average of  $\alpha$   
 381 based on the measured VOCs, the corresponding OH reaction rate constant and the  $\alpha$  (Table S1) in  
 382 Shanghai and Xinjin campaign, respectively. The model is initiated by the daytime averages of the  
 383 environmental parameters. A comparative analysis is conducted between the Xinjin campaign and the  
 384 Shanghai campaign where effective  $\alpha$  is determined to be 0.031 and 0.053, respectively. As illustrated  
 385 in Fig. 8a&b,  $P(O_3)$  exhibits a similar trend with the variations of  $NO_x$  and VOCs under different  $\alpha$ ,  
 386 while the value of  $P(O_3)$  reduces with larger  $\alpha$  at the same levels of precursors. For example, when  
 387 VOCs is at 8 ppbv and  $NO_x$  reaches 9 ppbv, the  $P(O_3)$  is 30.4 ppbv/h with  $\alpha$  of 0.031, whereas it  
 388 decreases to 24.6 ppbv/h when  $\alpha$  is 0.053. In addition, the larger of  $\alpha$  in the Shanghai campaign  
 389 increases the threshold of  $NO_x$  concentration for the transition of  $O_3$  production regime. When the  
 390 concentration of VOCs is fixed, a higher effective  $\alpha$  results in a lower  $NO_x$  concentration corresponding  
 391 to the peak of  $P(O_3)$ . Consequently, an increase in  $\alpha$  suppresses the peak of  $P(O_3)$  and simultaneously  
 392 affects its sensitivity to  $NO_x$  and VOCs concentrations.





394

395 **Figure 8.** Ozone production ( $P(O_3)$ , ppb h<sup>-1</sup>) derived from a simplified analytic model is plotted as a function of  $NO_x$   
 396 and VOCs under three different organic nitrate scenarios with branching ratios of (a) 0.031 for the Xinjin campaign,  
 397 (b) 0.053 for the Shanghai campaign, and (c) VOC-dependent branching ratios. ~~The for Shanghai campaign, where~~  
 398 ~~the branching ratio decreases linearly from 12 to 0.5% with VOCs from 100 to 5 ppbv (eas shown in (d)).~~

399 In the real atmosphere, the effective  $\alpha$  of ANs tends to exhibit a decline with the reduction of  
 400 VOCs concentration. Historical studies show the general range from 0.03 to 0.04 in rural sites and  
 401 from 0.04 to 0.10 in urban environments, depending on the composition of VOCs and the  $\alpha$  for BVOCs  
 402 (Farmer et al., 2011; Perring et al., 2010; Perring et al., 2013; Perring et al., 2009; Rosen et al., 2004b).  
 403 ~~The clean site referenced herein was selected as the baseline, corresponding to an  $\alpha$  value of 0.005~~  
 404 ~~when VOCs concentrations are less than 5 ppbv. In addition,  $\alpha$  was set at 0.12 when the VOCs~~  
 405 ~~concentration was 100 ppbv. The variation of  $\alpha$  related to VOCs concentration is shown in Fig. 8e. For~~  
 406 ~~simplicity, we use a linear relationship between  $\alpha$  and VOC concentration in the sensitivity analysis,~~  
 407 ~~as shown in Fig. 8d. An  $\alpha$  value of 0.005 was selected for clean condition with VOC concentration less~~  
 408 ~~than 5 ppbv, while 0.12 was selected for polluted condition with VOC concentration larger than 100~~  
 409 ~~ppbv. The lower limit of 0.005 is the average of the  $\alpha$  for methane and ethylene. The upper limit of~~  
 410 ~~0.12 is set as the reported value of the  $\alpha$  for isoprene and the  $\alpha$  for aromatic hydrocarbons are generally~~  
 411 ~~distributed around 0.1 (Perring et al., 2013). The assumption of this linear relationship between  $\alpha$  and~~  
 412 ~~VOC concentration has also been applied in a previous study (Farmer et al., 2011). With a varying  $\alpha$ ,~~  
 413 as shown in Fig. 8d,  $P(O_3)$  does not follow a consistent downward trend as VOCs decrease in VOC-  
 414 limited regime or transition regime. Instead, with the decrease of VOCs, the  $P(O_3)$  is likely to increase

带格式的: 字体颜色: 文字 1  
 带格式的: 字体颜色: 文字 1, 非上标/ 下标  
 带格式的: 字体颜色: 文字 1  
 带格式的: 字体颜色: 文字 1

415 at first at a relatively high VOCs distribution, and then decrease similar to the fixed  $\alpha$  scenario. Take  
416 the cases of the horizontal dashed line as an example, at a fixed  $\text{NO}_x$ , the  $\text{P}(\text{O}_3)$  ~~start to~~  
417 ~~increase~~increases, as the VOCs decrease ~~from 100 to~~within the range of about 60 to 100 ppbv,  
418 ~~and whereas~~  $\text{P}(\text{O}_3)$  subsequently decrease as VOCs ~~concentrations continue to decrease~~fell below 60  
419 ppbv. Therefore, ~~with the reduction in VOCs emission~~, an increase in  $\alpha$  directly correlates with a  
420 reduction in the  $\text{P}(\text{O}_3)$  peak. As a result, a positive correlation between  $\alpha$  and VOCs concentrations in  
421 real atmosphere might alter the  $\text{NO}_x$ -VOCs- $\text{O}_3$  relationship and diminish the effects of VOCs reduction  
422 on ozone control.

423 Scenarios with different VOCs reactivity and  $\alpha$  are selected for sensitivity tests to further  
424 investigate the impact of ANs ~~formation~~chemistry on the  $\text{O}_3$  pollution control strategy in Shanghai. As  
425 illustrated in Fig. 9a, variations of  $\text{P}(\text{O}_3)$  among three scenarios exhibit an initial increase followed  
426 by a subsequent decrease with rising  $\text{NO}_x$  ~~levels~~. For the typical ~~VOCs~~VOC reactivity and  $\alpha$  obtained  
427 from the Shanghai campaign, the ~~shift~~turning point from  $\text{NO}_x$  ~~disbenefit~~benefit to  $\text{NO}_x$  ~~limited~~limitation  
428 for  $\text{P}(\text{O}_3)$  ~~production~~ occurs at a  $\text{NO}_x$  concentration of 5.41.38 ppbv, when  $\text{P}(\text{O}_3)$  reaches a  
429 peak of 17.833.0 ppbv/h. When VOCs are reduced by 20% without accounting for the  
430 ~~changes~~reductions in  $\alpha$ , the ~~shift~~turning point for  $\text{NO}_x$  decreases to 4.91.26 ppbv with the  $\text{P}(\text{O}_3)$  peak  
431 of 16.3 ~~decreasing to~~decreasing to 30.1 ppbv/h. When the reduction of  $\alpha$  is considered ~~along with VOCs~~alongside  
432 ~~the decrease in VOCs~~ ( $\alpha$  decreases to 0.0270265), the peak of  $\text{P}(\text{O}_3)$  ~~at~~remains the ~~shift point~~turning point ~~increases~~  
433 by 5% ~~same as the initial case~~. Consequently, neglecting the ~~associated changes in~~may lead ~~changes~~is likely to an ~~overestimation of~~overestimate the effectiveness of emission control, ~~particularly in high~~  
434 ~~NO<sub>x</sub> environments~~. Our ~~observation~~showed~~observations~~ indicated that  $\text{NO}_x$  in Shanghai was notably  
435 high, which accords with the conditions ~~into~~ the right of the ~~shift~~turning point in Fig. 10. At 9a. In  
436 this ~~point~~case, the major chain-termination reaction ~~for~~of the  $\text{HO}_x$  cycle is the reaction between OH  
437 and  $\text{NO}_2$  to produce  $\text{HNO}_3$ , while the ~~production of~~share of the reaction that produces ANs  
438 ~~from~~through the reaction between  $\text{RO}_2$  and NO becomes relatively ~~small~~minor. As illustrated in Fig.  
439 9a, when  $\text{NO}_x$  changes from 22.0 to 1.0 ppbv, the impact of  $\alpha$  change will be larger, as the  $\text{P}(\text{O}_3)$   
440 difference between the two cases ranges from 0.1 to 2.6 ppbv/h. Therefore, the variation of  $\alpha$  has a  
441 ~~limited impact on~~impact ~~on~~of  $\text{O}_3$  production at high  $\text{NO}_x$ , whereas it offsets the impact of VOCs reduction as  $\text{NO}_x$   
442 decrease to around 1.5 ppbv which represents a low- $\text{NO}_x$  emission condition. In addition, the  
443 sensitivity analyses in a reduced VOC condition show that neglecting the  $\alpha$  change still overestimates  
444 the impact of VOCs reduction on  $\text{P}(\text{O}_3)$  by around 4 times with  $\text{NO}_x$  of 1 ppbv (Fig. 9b), which is also  
445 more significant than the case in Shanghai campaign. Therefore, the variation in  $\alpha$  has a temporarily  
446 limited impact on  $\text{O}_3$  production, whereas it should be seriously considered as  $\text{NO}_x$  levels continue to  
447 decrease.

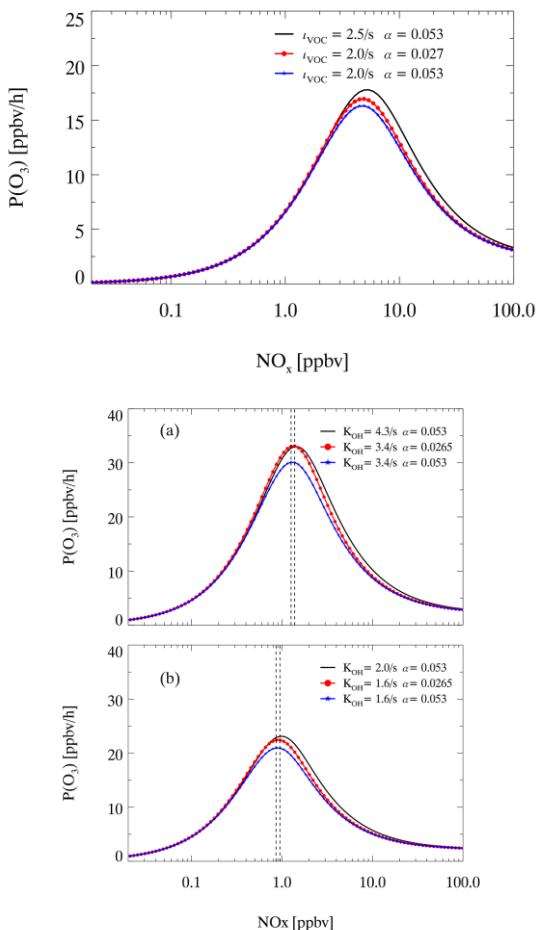


**Figure 9.** The ozone production rate ( $P(O_3)$ ) varies as a function of  $NO_x$  under different  $VOC-NO_x$  regimes for observed conditions during Shanghai campaign: (a) under mean measured parameters during the whole campaign (solid line, VOC reactivity ( $K_{OH}$ ) of 2.54.3/s, ANs branching ration ratio ( $\alpha$ ) of 0.053); a 20% reduction in VOC reactivity  $K_{OH}$  with a 50% reduction in branching ration  $\alpha$  (red dot line, 2.3.4/s, 0.0265); a 20% reduction in VOC reactivity  $K_{OH}$  with no change in branching ration  $\alpha$  (blue dot line, 2.3.4/s, 0.053). (b) under observed parameters during the clean days (solid line,  $K_{OH}$  of 2.0/s,  $\alpha$  of 0.053); a 20% reduction in  $K_{OH}$  with a 50% reduction in  $\alpha$  (red dot line, 1.6/s, 0.0265); a 20% reduction in  $K_{OH}$  with no change in  $\alpha$  (blue dot line, 1.6/s, 0.053). Dash lines show the turning point in different cases.

To further investigate the effect of ANs formation on O<sub>3</sub> production during different days, sensitivity tests on VOCs reactivity and  $\alpha$  are conducted based on typical conditions during different periods. The  $\alpha$  values are derived as 0.055, 0.054 and 0.052, for the high ozone, clean and background

462 periods, respectively. As shown in Fig. S4, the  $P(O_3)$  exhibits a similar trend with the increase of  $NO_x$   
463 across different periods. The  $P(O_3)$  peak during the background period (30.3 ppbv/h) is slightly lower  
464 than that during both the high ozone days and the clean days (32.5 and 32.4 ppbv/h). Therefore, the  
465 ANs chemistry has similar effects on  $O_3$  production within different periods during the Shanghai  
466 campaign. Further comparisons of ozone production under varying precursor levels were conducted  
467 using historical observations collected in August 1994 at Mecklenburg-Vorpommern Mankmoos (MK),  
468 Germany (Ehhalt, 1999), and during the spring of 2006 in Mexico City (MX) (Farmer et al., 2011;  
469 Perring et al., 2010). The MK site serves as a typical clean background location with a very low  
470 effective  $\alpha$  of 0.005, corresponding to  $\tau VOC$  of  $0.4\text{ s}^{-1}$ , where methane is the predominant pollutant.  
471 Conversely, the MX site is characterized as an urban environment with an effective  $\alpha$  of 0.036, where  
472 a total of 58 VOCs was measured, corresponding to  $\tau VOC$  of  $3.1\text{ s}^{-1}$ . The MK site shows a peak of  
473  $P(O_3)$  is 2.2 ppbv/h at the  $NO_x$  of 0.63 ppbv. In contrast, the MX site demonstrates a peak  $P(O_3)$  of 7.2  
474 ppbv/h at a  $NO_x$  of 1.9 ppbv. Given that the Xinjin and Shanghai sites exhibit higher VOCs reactivity  
475 than MX, the corresponding peak  $P(O_3)$  and the  $NO_x$  inflection point are significantly elevated. This  
476 increase is primarily attributed to the high  $P(HO_x)$ , coupled with a low  $\alpha$ , which substantially enhances  
477  $P(O_3)$  under the intensified  $HO_x$  cycling. Consequently, the ozone production potentials of urban sites  
478 in China are overall higher than in other regions, while the influence of  $\alpha$  appears to be weak.

#### 479 4. Conclusions

480 This study reveals the abundances of PNs and ANs and quantifies their respective impacts on  $O_3$   
481 pollution based on the field campaign in Shanghai. They both showed higher values but less  
482 pronounced diurnal variation during the  $O_3$  pollution period than the clean period. The mechanism  
483 validation indicates that Berkeley mechanism generally outperforms in the simulation of organic  
484 nitrates. The ratio of  $PNs/O_3$  serves as a significant indicator of photochemistry. In comparison to the  
485 previous Xinjin campaign, the inhibition effect of PNs chemistry on daytime  $O_3$  production diminished,  
486 likely attributed to the lower production of PNs. For ANs, the model simulation demonstrated that the  
487 branching ratio ( $\alpha$ ) influences the  $NO_x$ -VOCs- $O_3$  sensitivity. The consideration of  $\alpha$  value not only  
488 alters the  $P(O_3)$  peak in EKMA but also resulted in low effectiveness of precursor reductions, as the  $\alpha$   
489 would change with the reduction of VOCs. It is worth mentioning that the complex polluted regions  
490 are usually characterized by high  $NO_x$  and  $HO_x$ . In that case, the contribution of chain-termination  
491 reactions that produce ANs could be reduced, leading to limited impact of AN chemistry on  $O_3$   
492 formation. The effect of ANs chemistry on  $O_3$  pollution control is therefore expected to enhance with  
493 further precursor reductions, and we suggest a pressing need for more measurements and analysis of  
494 organic nitrates to address the forthcoming challenges in air pollution mitigation.

495  
496 **Code/Data availability.** The datasets used in this study are available from the corresponding author  
497 upon request (chenxr95@mail.sysu.edu.cn; k.lu@pku.edu.cn).

498  
499 **Author contributions.** K.D.L. and X.R.C. designed the study. C.M.L. and X.R.C. analyzed the data  
500 and wrote the paper with input from K.D.L.

501  
502 **Competing interests.** The authors declare that they have no conflicts of interest.

---

504 **Acknowledgments.** This work was supported by the National Natural Science Foundation of China  
505 (Grants No. 42407139); the National Natural Science Foundation of China (Grants No. 22406204);  
506 the special fund of State Environmental Protection Key Laboratory of Formation and Prevention of  
507 Urban Air Pollution Complex (SEPAir-2024080219); the Innovative Exploration Program of National  
508 Institute of Metrology, China (No. AKYCX2313).

509

## 510 References

511 Arey J, Aschmann SM, Kwok ESC, Atkinson R. Alkyl Nitrate, Hydroxyalkyl Nitrate, and Hydroxycarbonyl Formation  
512 from the NO<sub>x</sub>–Air Photooxidations of C5–C8 n-Alkanes. *The Journal of Physical Chemistry A* 2001; 105: 1020-  
513 1027.

514 Aruffo E, Di Carlo P, Dari-Salisburgo C, Biancofiore F, Giammaria F, Busilacchio M, et al. Aircraft observations of the  
515 lower troposphere above a megacity: Alkyl nitrate and ozone chemistry. *Atmospheric Environment* 2014; 94: 479-  
516 488.

517 Ashmore MR. Assessing the future global impacts of ozone on vegetation. *Plant Cell and Environment* 2005; 28: 949-964.

518 Browne EC, Cohen RC, Wooldridge PJ, Valin LC, Min K-E. Organic nitrate formation: Impacts on NO<sub>x</sub> lifetime and ozone.  
519 Abstracts of Papers of the American Chemical Society 2012; 244.

520 Browne EC, Min KE, Wooldridge PJ, Apel E, Blake DR, Brune WH, et al. Observations of total RONO<sub>2</sub> over the boreal  
521 forest: NO<sub>x</sub> sinks and HNO<sub>3</sub> sources. *Atmospheric Chemistry and Physics* 2013; 13: 4543-4562.

522 Chen J, Wu H, Liu AW, Hu SM, Zhang J. Field Measurement of NO<sub>2</sub> and RNO<sub>2</sub> by Two-Channel Thermal Dissociation  
523 Cavity Ring Down Spectrometer. *Chinese Journal of Chemical Physics* 2017; 30: 493-498.

524 Darer AI, Cole-Filiplak NC, O'Connor AE, Elrod MJ. Formation and Stability of Atmospherically Relevant Isoprene-  
525 Derived Organosulfates and Organonitrates. *Environmental Science & Technology* 2011; 45: 1895-1902.

526 Day DA, Dillon MB, Wooldridge PJ, Thornton JA, Rosen RS, Wood EC, et al. On alkyl nitrates, O<sub>3</sub>, and the "missing  
527 NO<sub>y</sub>". *Journal of Geophysical Research-Atmospheres* 2003; 108.

528 Ehhalt DH. Photooxidation of trace gases in the troposphere. *Physical Chemistry Chemical Physics* 1999; 1: 5401-5408.

529 Farmer DK, Perring AE, Wooldridge PJ, Blake DR, Baker A, Meinardi S, et al. Impact of organic nitrates on urban ozone  
530 production. *Atmospheric Chemistry and Physics* 2011; 11: 4085-4094.

531 Fisher JA, Jacob DJ, Travis KR, Kim PS, Marais EA, Miller CC, et al. Organic nitrate chemistry and its implications for  
532 nitrogen budgets in an isoprene- and monoterpane-rich atmosphere: constraints from aircraft (SEAC4RS) and  
533 ground-based (SOAS) observations in the Southeast US. *Atmospheric Chemistry and Physics* 2016; 16: 5969-5991.

534 Flocke F, Volz-Thomas A, Buers HJ, Patz W, Garthe HJ, Kley D. Long-term measurements of alkyl nitrates in southern  
535 Germany I. General behavior and seasonal and diurnal variation. *Journal of Geophysical Research-Atmospheres* 1998;  
536 103: 5729-5746.

537 Gao W, Tie X, Xu J, Huang R, Mao X, Zhou G, et al. Long-term trend of O<sub>3</sub> in a mega City (Shanghai), China:  
538 Characteristics, causes, and interactions with precursors. *Science of the Total Environment* 2017; 603: 425-433.

539 Grosjean E, Grosjean D, Woodhouse LF, Yang YJ. Peroxyacetyl nitrate and peroxypropionyl nitrate in Porto Alegre, Brazil.  
540 Atmospheric Environment 2002; 36: 2405-2419.

541 Ito A, Sillman S, Penner JE. Global chemical transport model study of ozone response to changes in chemical kinetics and  
542 biogenic volatile organic compounds emissions due to increasing temperatures: Sensitivities to isoprene nitrate  
543 chemistry and grid resolution. *Journal of Geophysical Research-Atmospheres* 2009; 114.

544 Lee G, Jang Y, Lee H, Han J-S, Kim K-R, Lee M. Characteristic behavior of peroxyacetyl nitrate (PAN) in Seoul megacity,  
545 Korea. *Chemosphere* 2008; 73: 619-628.

546 Li C, Wang H, Chen X, Zhai T, Chen S, Li X, et al. Thermal dissociation cavity-enhanced absorption spectrometer for  
547 measuring NO<sub>2</sub>, RO<sub>2</sub>NO<sub>2</sub>, and RONO<sub>2</sub> in the atmosphere. *Atmospheric Measurement Techniques* 2021; 14: 4033-  
548 4051.

549 Li C, Wang H, Chen X, Zhai T, Ma X, Yang X, et al. Observation and modeling of organic nitrates on a suburban site in  
550 southwest China. *Science of the Total Environment* 2023; 859.

551 Liebmann J, Karu E, Sobanski N, Schuladen J, Ehn M, Schallhart S, et al. Direct measurement of NO<sub>3</sub> radical reactivity  
552 in a boreal forest. *Atmospheric Chemistry and Physics* 2018; 18: 3799-3815.

553 Liebmann J, Sobanski N, Schuladen J, Karu E, Hellen H, Hakola H, et al. Alkyl nitrates in the boreal forest: formation via  
554 the NO<sub>3</sub>-, OH- and O<sub>3</sub>-induced oxidation of biogenic volatile organic compounds and ambient lifetimes.  
555 *Atmospheric Chemistry and Physics* 2019; 19: 10391-10403.

556 Ling ZH, Guo H, Simpson IJ, Saunders SM, Lam SHM, Lyu XP, et al. New insight into the spatiotemporal variability and  
557 source apportionments of C<sub>1</sub>-C<sub>4</sub> alkyl nitrates in Hong Kong. *Atmospheric Chemistry and Physics* 2016; 16: 8141-  
558 8156.

559 Liu Y, Shen H, Mu J, Li H, Chen T, Yang J, et al. Formation of peroxyacetyl nitrate (PAN) and its impact on ozone  
560 production in the coastal atmosphere of Qingdao, North China. *Science of the Total Environment* 2021; 778.

561 Lu KD, Hofzumahaus A, Holland F, Bohn B, Brauers T, Fuchs H, et al. Missing OH source in a suburban environment near  
562 Beijing: observed and modelled OH and HO<sub><sub>2</sub></sub> concentrations in summer 2006. *Atmospheric  
563 Chemistry and Physics* 2013; 13: 1057-1080.

564 Monks PS, Archibald AT, Colette A, Cooper O, Coyle M, Derwent R, et al. Tropospheric ozone and its precursors from the  
565 urban to the global scale from air quality to short-lived climate forcer. *Atmos. Chem. Phys.* 2015; 15: 8889-8973.

566 Ng NL, Brown SS, Archibald AT, Atlas E, Cohen RC, Crowley JN, et al. Nitrate radicals and biogenic volatile organic

567 compounds: oxidation, mechanisms, and organic aerosol. *Atmospheric Chemistry and Physics* 2017; 17: 2103-2162.

568 Perring AE, Bertram TH, Farmer DK, Wooldridge PJ, Dibb J, Blake NJ, et al. The production and persistence of Sigma

569 RONO<sub>2</sub> in the Mexico City plume. *Atmospheric Chemistry and Physics* 2010; 10: 7215-7229.

570 Perring AE, Pusede SE, Cohen RC. An Observational Perspective on the Atmospheric Impacts of Alkyl and Multifunctional

571 Nitrates on Ozono and Secondary Organic Aerosol. *Chemical Reviews* 2013; 113: 5848-5870.

572 Perring AE, Wisthaler A, Graus M, Wooldridge PJ, Lockwood AL, Mielke LH, et al. A product study of the isoprene+NO<sub>3</sub>

573 reaction. *Atmospheric Chemistry and Physics* 2009; 9: 4945-4956.

574 Present PSR, Zare A, Cohen RC. The changing role of organic nitrates in the removal and transport of NO<sub>x</sub>. *Atmospheric*

575 *Chemistry and Physics* 2020; 20: 267-279.

576 Reisen F, Aschmann SM, Atkinson R, Arey J. 1,4-hydroxycarbonyl products of the OH radical initiated reactions of C-5-

577 C-8 n-alkanes in the presence of NO<sub>x</sub>. *Environmental Science & Technology* 2005; 39: 4447-4453.

578 Roberts JM, Bertman SB. The thermal-decomposition of peroxyacetic nitric anhydride (pan) and peroymethacrylic nitric

579 anhydride (MPAN). *International Journal of Chemical Kinetics* 1992; 24: 297-307.

580 Romer PS, Duffey KC, Wooldridge PJ, Allen HM, Ayres BR, Brown SS, et al. The lifetime of nitrogen oxides in an

581 isoprene-dominated forest. *Atmospheric Chemistry and Physics* 2016; 16: 7623-7637.

582 Romer PS, Duffey KC, Wooldridge PJ, Edgerton E, Baumann K, Feiner PA, et al. Effects of temperature-dependent NO<sub>x</sub>

583 emissions on continental ozone production. *Atmospheric Chemistry and Physics* 2018; 18: 2601-2614.

584 Rosen RS, Wood EC, Wooldridge PJ, Thornton JA, Day DA, Kuster W, et al. Observations of total alkyl nitrates during

585 Texas Air Quality Study 2000: Implications for O<sub>3</sub> and alkyl nitrate photochemistry. *Journal of Geophysical*

586 *Research-Atmospheres* 2004a; 109: 15.

587 Rosen RS, Wood EC, Wooldridge PJ, Thornton JA, Day DA, Kuster W, et al. Observations of total alkyl nitrates during

588 Texas Air Quality Study 2000: Implications for O<sub>3</sub> and alkyl nitrate photochemistry. *Journal of Geophysical*

589 *Research-Atmospheres* 2004b; 109.

590 Sadanaga Y, Takaji R, Ishiyama A, Nakajima K, Matsuki A, Bandow H. Thermal dissociation cavity attenuated phase shift

591 spectroscopy for continuous measurement of total peroxy and organic nitrates in the clean atmosphere. *Review of*

592 *Scientific Instruments* 2016; 87.

593 Schwantes RH, Emmons LK, Orlando JJ, Barth MC, Tyndall GS, Hall SR, et al. Comprehensive isoprene and terpene gas-

594 phase chemistry improves simulated surface ozone in the southeastern US. *Atmospheric Chemistry and Physics* 2020;

595 20: 3739-3776.

596 Shepson PB, Hastic DR, So KW, Schiff HI. Relationships between PAN, PPN and O<sub>3</sub> at urban and rural sites in Ontario.

597 *Atmospheric Environment Part a-General Topics* 1992; 26: 1259-1270.

598 Song J, Zhang Y, Huang Y, Ho KF, Yuan Z, Ling Z, et al. Seasonal variations of C-1-C-4 alkyl nitrates at a coastal site in

599 Hong Kong: Influence of photochemical formation and oceanic emissions. *Chemosphere* 2018; 194: 275-284.

600 Sun J, Li Z, Xue L, Wang T, Wang X, Gao J, et al. Summertime C-1-C-5 alkyl nitrates over Beijing, northern China: Spatial

601 distribution, regional transport, and formation mechanisms. *Atmospheric Research* 2018; 204: 102-109.

602 Sun M, Cui Jn, Zhao X, Zhang J. Impacts of precursors on peroxyacetyl nitrate (PAN) and relative formation of PAN to

603 ozone in a southwestern megacity of China. *Atmospheric Environment* 2020; 231.

604 Tan Z, Fuchs H, Lu K, Hofzumahaus A, Bohn B, Broch S, et al. Radical chemistry at a rural site (Wangdu) in the North

605 China Plain: observation and model calculations of OH, HO<sub>2</sub> and RO<sub>2</sub> radicals. *Atmos. Chem. Phys.* 2017a; 17: 663-

606 690.

607 Tan Z, Fuchs H, Lu K, Hofzumahaus A, Bohn B, Broch S, et al. Radical chemistry at a rural site (Wangdu) in the North

608 China Plain: observation and model calculations of OH, HO<sub>2</sub> and RO<sub>2</sub> radicals. *Atmospheric Chemistry and Physics* 2017b; 17: 663-690.

609 Tan Z, Lu K, Jiang M, Su R, Dong H, Zeng L, et al. Exploring ozone pollution in Chengdu, southwestern China: A case

610 study from radical chemistry to O<sub>3</sub>-VOC-NO<sub>x</sub> sensitivity. *Sci Total Environ* 2018a; 636: 775-786.

611 Tan ZF, Rohrer F, Lu KD, Ma XF, Bohn B, Broch S, et al. Wintertime photochemistry in Beijing: observations of RO<sub>x</sub>

612 radical concentrations in the North China Plain during the BEST-ONE campaign. *Atmospheric Chemistry and Physics*

613 2018b; 18: 12391-12411.

614 Teng AP, Crounse JD, Lee L, St Clair JM, Cohen RC, Wennberg PO. Hydroxy nitrate production in the OH-initiated

615 oxidation of alkenes. *Atmospheric Chemistry and Physics* 2015; 15: 4297-4316.

616 Travis KR, Jacob DJ, Fisher JA, Kim PS, Marais EA, Zhu L, et al. Why do models overestimate surface ozone in the

617 Southeast United States? *Atmospheric Chemistry and Physics* 2016; 16: 13561-13577.

618 Wang M, Shao M, Chen W, Lu S, Wang C, Huang D, et al. Measurements of C1-C4 alkyl nitrates and their relationships

619 with carbonyl compounds and O<sub>3</sub> in Chinese cities. *Atmospheric Environment* 2013; 81: 389-398.

620 Wang W, Parrish DD, Wang S, Bao F, Ni R, Li X, et al. Long-term trend of ozone pollution in China during 2014-2020:

621 distinct seasonal and spatial characteristics and ozone sensitivity. *Atmospheric Chemistry and Physics* 2022; 22: 8935-

622 8949.

623

624 Xu T, Nie W, Xu Z, Yan C, Liu Y, Zha Q, et al. Investigation on the budget of peroxyacetyl nitrate (PAN) in the Yangtze  
625 River Delta: Unravelling local photochemistry and regional impact. *Science of the Total Environment* 2024; 917.

626 Xue K, Zhang X. The rationale behind updates to ambient ozone guidelines and standards. *Frontiers in Public Health* 2023;  
627 11.

628 Yeh GK, Ziemann PJ. Alkyl Nitrate Formation from the Reactions of C<sub>8</sub>-C<sub>14</sub>-*n*-Alkanes  
629 with OH Radicals in the Presence of NO<sub>x</sub>: Measured Yields with Essential Corrections for Gas-  
630 Wall Partitioning. *Journal of Physical Chemistry A* 2014a; 118: 8147-8157.

631 Yeh GK, Ziemann PJ. Identification and Yields of 1,4-Hydroxynitrates Formed from the Reactions of C<sub>8</sub>-  
632 C<sub>16</sub>-*n*-Alkanes with OH Radicals in the Presence of NO<sub>x</sub>. *Journal of Physical Chemistry A* 2014b; 118: 8797-8806.

633 Young PJ, Naik V, Fiore AM, Gaudel A, Guo J, Lin MY, et al. Tropospheric Ozone Assessment Report: Assessment of  
634 global-scale model performance for global and regional ozone distributions, variability, and trends. *Elementa-Science  
635 of the Anthropocene* 2018; 6.

636 Zare A, Romer PS, Tran N, Keutsch FN, Skog K, Cohen RC. A comprehensive organic nitrate chemistry: insights into the  
637 lifetime of atmospheric organic nitrates. *Atmospheric Chemistry and Physics* 2018; 18: 15419-15436.

638 Zeng L, Fan G-J, Lyu X, Guo H, Wang J-L, Yao D. Atmospheric fate of peroxyacetyl nitrate in suburban Hong Kong and  
639 its impact on local ozone pollution. *Environmental Pollution* 2019; 252: 1910-1919.

640 Zhang B, Zhao X, Zhang J. Characteristics of peroxyacetyl nitrate pollution during a 2015 winter haze episode in Beijing.  
641 *Environmental Pollution* 2019; 244: 379-387.

642 Zhang G, Xia L, Zang K, Xu W, Zhang F, Liang L, et al. The abundance and inter-relationship of atmospheric peroxyacetyl  
643 nitrate (PAN), peroxypropionyl nitrate (PPN), O<sub>3</sub>, and NO<sub>y</sub> during the wintertime in Beijing, China. *Science of the  
644 Total Environment* 2020; 718.

645 Zhang H, Tong S, Zhang W, Xu Y, Zhai M, Guo Y, et al. A comprehensive observation on the pollution characteristics of  
646 peroxyacetyl nitrate (PAN) in Beijing, China. *Science of the Total Environment* 2023; 905.

647 Zhang H, Xu X, Lin W, Wang Y. Wintertime peroxyacetyl nitrate (PAN) in the megacity Beijing: Role of photochemical  
648 and meteorological processes. *Journal of Environmental Sciences* 2014; 26: 83-96.

649 Zhang JM, Wang T, Ding AJ, Zhou XH, Xue LK, Poon CN, et al. Continuous measurement of peroxyacetyl nitrate (PAN)  
650 in suburban and remote areas of western China. *Atmospheric Environment* 2009; 43: 228-237.

651 Zhu W, Zhou M, Cheng Z, Yan N, Huang C, Qiao L, et al. Seasonal variation of aerosol compositions in Shanghai, China:  
652 Insights from particle aerosol mass spectrometer observations. *Science of The Total Environment* 2021; 771: 144948.

653

654